



Tracing shock waves: type II radio emission on 27th of September 2001

Firas Al-Hamadani¹ · Amjad Al-Sawad²

Received: 2 December 2023 / Accepted: 18 June 2024
© The Author(s), under exclusive licence to Springer Nature B.V. 2024

Abstract

This study focus on atypical Type II radio bursts observed in conjunction with three simultaneous coronal mass ejections (CMEs) on September 27, 2001. These CMEs originated from a single active region (AR) and were linked to relatively weak solar flares. Analysis of the CME sequences revealed distinct periods of interplanetary (IP) Type II radio emissions, characterized by pronounced increases in intensity. The first radio enhancement, lasting 20 minutes, exhibited very low density and frequency (1.65–1.5 MHz) at a height range of (7.8–8.2) solar radii (R_{\odot}). Subsequently, the second radio signature persisted for 40 minutes with a frequency range of (900–700) kHz and a height range of (10.9–12.6) R_{\odot} . The third radio signature spanned 1 hour and 20 minutes, featuring a frequency range of (660–390) kHz and a height range of (13.2–18.6) R_{\odot} . The fourth enhancement extended over 3 hours, ranging from (550–250) kHz in frequency and (14.6–25.0) R_{\odot} in height. We concluded that the initial low-density radio signature resulted from a shock wave generated by reconnection of magnetic field lines, without an intense flare or extreme ultraviolet imaging telescope (EIT) wave. This shock wave then accelerated subsequent CMEs. Alternatively, the radio burst could have formed in the wake of the initial slow CME, creating a low-density environment. The second radio enhancement coincided with the accelerated propagation of CME1's core and was attributed to enhanced radio emission resulting from the Type II shock encountering filament material. The third radio enhancement aligned with the concept of a CME bow shock, indicating that the shock was positioned at the leading front of the CME. This enhancement occurred when the shock met remnant material from earlier CMEs, yet the shock continued propagating at a constant speed. The fourth enhancement progressed to higher frequencies due to the merging of CME1's core with CME2, propagating along CME3's path. This comprehensive analysis provides valuable insights into the complex dynamics and interactions associated with these unique Type II radio bursts and their correlation with coronal mass ejections.

Keywords Coronal mass ejections · Initiation and propagation · Radio bursts · Meter-wavelengths and longer (m, dkm, hm, km) · Type II

1 Introduction

Plasma clouds, magnetized and expelled from the solar corona into IP space, are recognized as CMEs (Webb and Howard 2012). Particularly when directed towards Earth, CMEs possess the capability to induce significant disruptions in space weather. This fact underscores their impor-

tance (Webb and Howard 2012). Energetic solar events, including solar flares, frequently accompany CMEs and give rise to solar radio bursts. These events stimulate electron beams through a plasma emission mechanism, ultimately generating radio wavelength emissions (Klassen et al. 2002).

Solar radio bursts are classified into types I–V according to their characteristics and dynamic spectral shapes (Wild 1963). Types II and IV bursts, unlike type I bursts, are seldom associated with solar flares alone, often being linked to either a CME and a flare or solely a CME (Kumar et al. 2016). Metric type II bursts, occurring at high frequencies, result from flare shocks (Gary et al. 1984) while CME-driven shocks produce IP Type II radio emissions at low frequencies (Cane et al. 1987). Decameter-hectometric (DH) type II radio emissions, indicative of potent magnetohydrodynamic (MHD) shocks emerging from the inner solar

✉ A. Al-Sawad
aalsawad@yahoo.com

F. Al-Hamadani
firas.balbool@uobasrah.edu.iq

¹ Department of physics, college of sciences, University of Basrah, Basrah, Iraq

² Ministry of Higher Education and Scientific Research, Baghdad, Iraq

corona, propagate within the IP medium (Gopalswamy et al. 2000).

Typically, type II radio bursts exhibit a dual-band emission spectrum, featuring a fundamental and harmonic emission band. The fundamental frequency corresponds to the plasma frequency of the emission region, gradually decreasing as the coronal shock progresses outward into the heliosphere (Cane et al. 1987; Gopalswamy et al. 2000). Band splitting, often considered a consequence of plasma emission from upstream and downstream shock regions, is also observed (Smerd et al. 1975). Type II radio bursts, primarily caused by shocks traversing the lower solar corona, typically occur at or below 100 MHz. Those in the decimeter and kilometer wavelength range result from shocks passing through the upper corona and IP space. Monitoring type II radio bursts facilitates estimating the time of disturbances caused by CMEs reaching Earth (Cremades et al. 2007).

While this event has been previously investigated (Al-Hamadani and Pohjolainen 2017), our study expands on earlier analyses. In Sect. 4, utilizing LASCO coronagraph data, we demonstrate that type II radio emissions commence late and at very low frequencies, concurrently associated with three CMEs. Section 3 explores the associated solar flare. Section 5 delves into the sequential events, revealing four distinct time periods of IP type II radio emission with pronounced enhancements in intensity. Section 6 discusses atmospheric density models and their role in estimating the heights of type II bursts, comparing them with CME heights. Finally, Sect. 7 provides a detailed analysis of the arrival shock wave.

2 Data analysis

White-light observations and their characteristics were extracted from the Large Angle and Spectrometric Coronagraph Experiment (LASCO) on the Solar and Heliospheric Observatory (SOHO). For cataloging the data on IP radio type II events, the Radio and Plasma Wave Experiment (WAVES) on the Wind spacecraft was employed (Bougeret et al. 1995). Flare data were sourced from the National Oceanic and Atmospheric Administration (NOAA). Solar x-ray fluxes were monitored using the Geostationary Operational Environmental Satellite (GOES), while x-ray imaging was facilitated by the Yohkoh soft x-ray telescope (SXT; (Tsuneta et al. 1991). To investigate structures in extreme ultraviolet (EUV), SOHO's Extreme-Ultraviolet Imaging Telescope (EIT; (Delaboudinière et al. 1995) images were utilized. H α images were obtained from the Kanzelhöhe Solar Observatory, courtesy of the Global High-Resolution H-alpha Network. To assess the proximity of shock waves to Earth, three spacecraft were employed: the Advanced Composition Explorer (ACE), Wind, and the Charge, Element,

and Isotope Analysis System (CELIAS) on board SOHO. The calculation of radio source heights aimed to compare them with CME heights and radio enhancement heights. This comprehensive array of data sources ensures a robust and multifaceted approach to investigating the phenomena under study.

3 Solar flares

Several small H α flares were observed in NOAA active region (AR) 9628 from September 26 at 23:07 to September 27 at 8:23 UT. Yohkoh soft x-ray telescope (SXT) disk images at 06:07 and 10:04 UT revealed a complex active region system near the solar limb's southwestern edge (see Fig. 1).

There was no substantial amount of heated plasma in the region where the flare occurred at lower altitudes. The occurrence of CMEs during a period of weak solar flare activity is intriguing. This observation suggests the possibility of magnetic reconnection at higher levels of the corona during that time, as the corona did not exhibit the typical signs of a solar flare.

4 Coronal mass ejections

Given that the first coronal mass ejection (CME1) and the third CME (CME3) were both detected in the same direction (200 degrees south) according to the LASCO catalog. While the second CME (CME2) was situated further west (240 degrees), an initial impression might suggest that CME2 and CME3 could be components of the same event. The distinction between the fronts of CME2 and CME3 is challenging, and variations in reported heights could be attributed to different measurement inclinations. Consequently, a plausible interpretation emerges, considering CME2 and CME3 as two separate loops that may appear connected due to their proximity within the same CME event. However, a more detailed analysis revealed otherwise; CME2 and CME3 are distinct events, as confirmed through a comprehensive examination of all LASCO images and reported heights (see Fig. 8).

At 08:20 UT, when the IP Type II radio emissions commenced, CME1 exhibited a southward propagation, with a leading front height of 12.1 R_{\odot} and a propagation speed of approximately 340 km s $^{-1}$. CME1 displayed a characteristic structure (refer to Fig. 2) with a bright front, followed by a cavity and a bright core. The core's heights were also calculated, reaching 8.49 R_{\odot} at 08:18 UT, with an estimated propagation speed of around 220 km s $^{-1}$. We conducted measurements of the projected heights of the CME1 core as a function of time. The initial measurement was taken where the core was observed at a height of 2.8 R_{\odot}

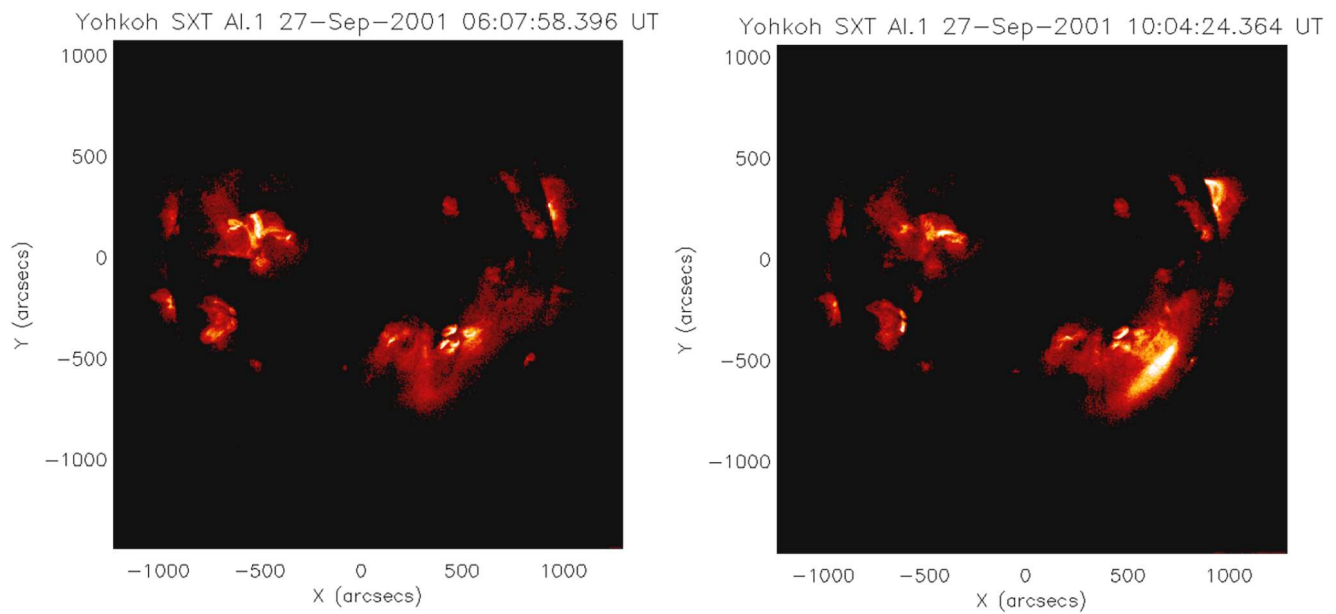
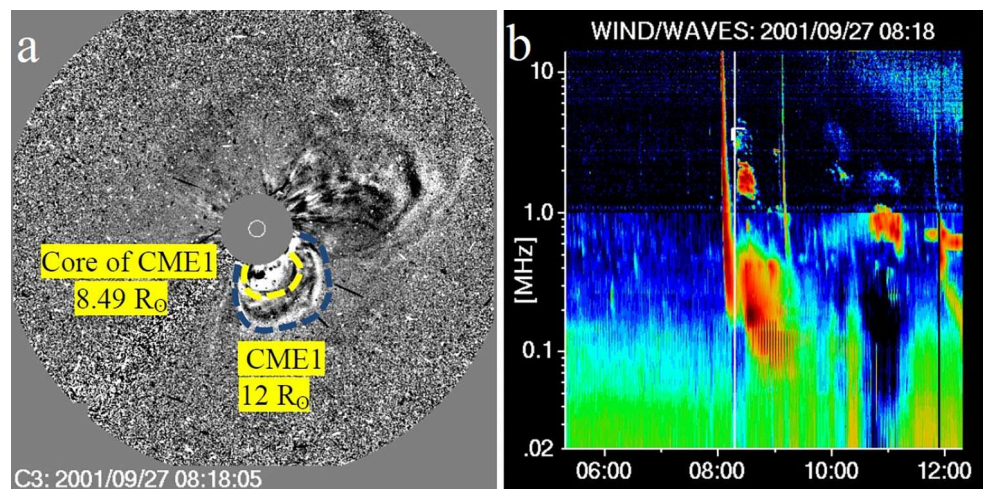


Fig. 1 The Yohkoh/SXT full-disk soft X-ray images at 06:07 UT (left) and 10:04 UT (right)

Fig. 2 The Fig 2a: At 08:18 UT on 27 September 2001 the CME1 leading front was followed by a cavity and a core. The leading front is marked with a dashed blue line and the core with a dashed yellow line. Fig 2b: Wind WAVES radio spectrum shows the first radio type II burst enhancement. The radio emission frequency used for the height calculation is 1.65 MHz which indicates a source height of about $7.8 R_{\odot}$ (hybrid atmospheric density model) close to leading front of the CME1 core height $8.49 R_{\odot}$



Subsequently, we tracked the core up to approximately $30 R_{\odot}$ (at 14:42 UT). Notably, by 10:20 UT, the CME1 core had partially merged with the core of CME2, forming a bright front in the plane of the sky. The third, faster CME seemed to propel the previous two forward. Initially, the CME1 core exhibited a speed below 100 km s^{-1} , but similar to the leading front, it accelerated and reached approximately 350 km s^{-1} by 09:40 UT. Surprisingly, it then experienced a much stronger acceleration, ultimately reaching its final speed of about 1000 km s^{-1} by 14:42 UT.

This detailed analysis clarifies (as illustrated in Fig. 8) the individual characteristics and trajectories of CME1, CME2, and CME3 during the observed event.

Following CME1, CME2 propagated southwestward with a central propagation angle of 246 degrees, as depicted in Fig. 3. Initially, CME2 exhibited a relatively slow speed,

accelerating around the onset of the IP Type II burst. Its heights were recorded at $4.4 R_{\odot}$ at 07:54 UT and $5.0 R_{\odot}$ at 08:30 UT, corresponding to a speed of approximately 200 km s^{-1} . As it reached a height of around $30 R_{\odot}$, its speed surged to about 1000 km s^{-1} .

Figure 4 shows the positions of CME1 leading front (dashed blue line), CME1 core (dashed yellow line), CME2 leading front (dashed red line), and CME3 leading front (dashed purple line) at 10:42 UT. Post this snapshot, the CME1 leading front is no longer visible, aligning with the commencement of the second type II radio enhancement. The radio emission source height coincided at approximately $10.9 R_{\odot}$ (900 kHz), closely mirroring the height of the CME2 leading front ($11.9 R_{\odot}$).

A third partial halo CME (CME3) emerged at 08:30 UT, initially observed at a height of $4.2 R_{\odot}$. Positioned at a cen-

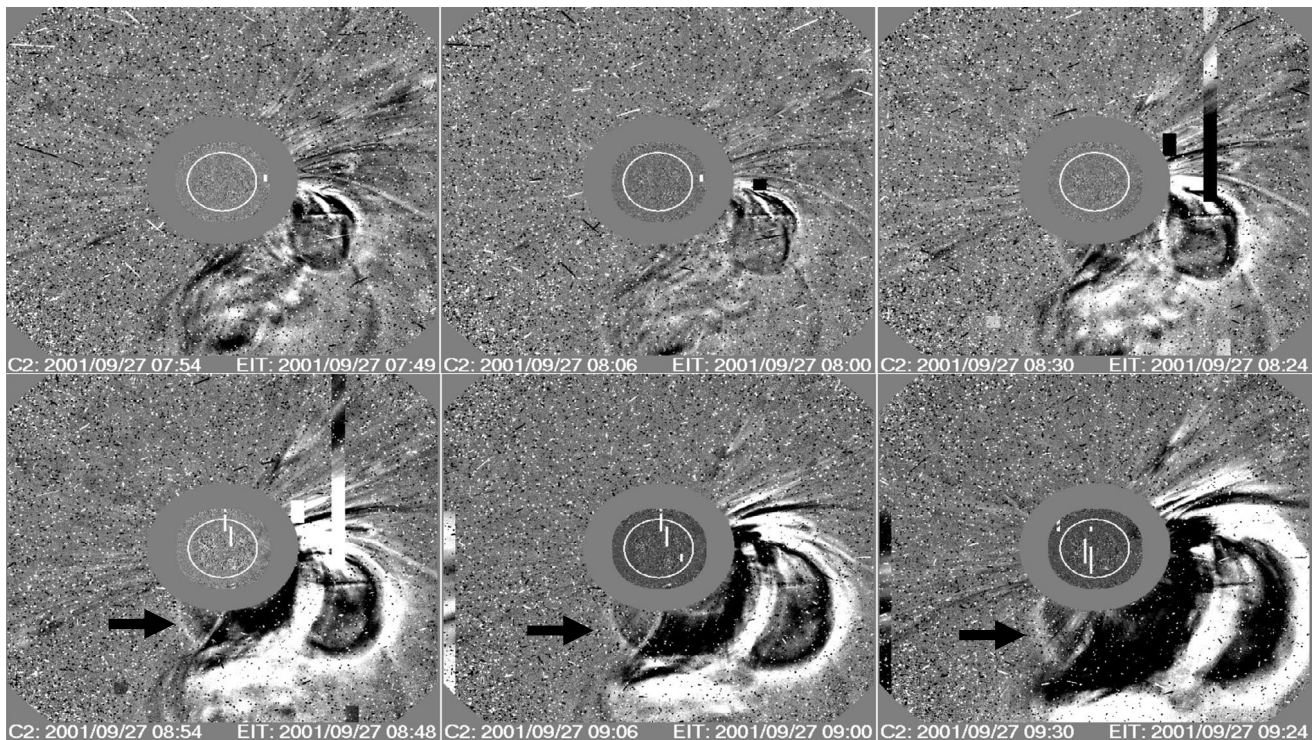
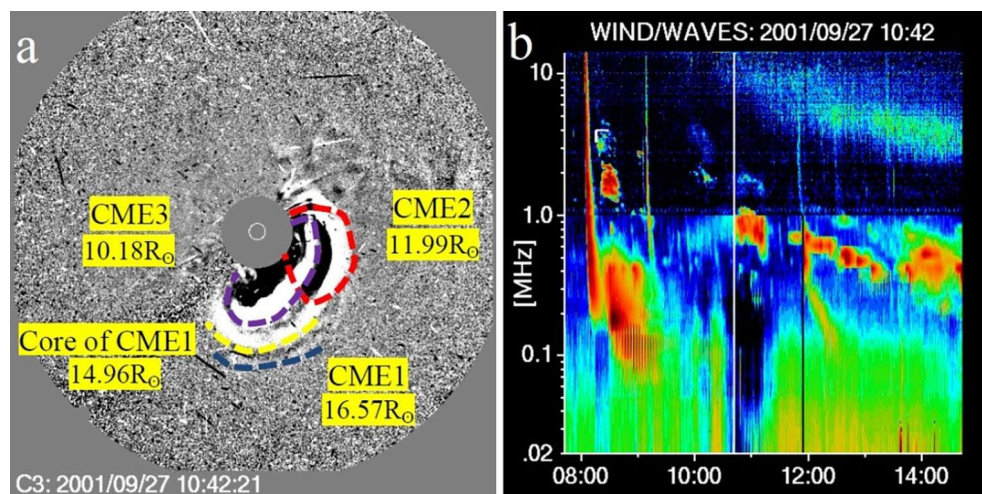


Fig. 3 Early evolution of CME2 and CME3 on 27 September 2001. The start of the radio type II emission occurred at 08:20 UT, in between the second (08:06 UT) and third (08:30 UT) LASCO C2 image.

CME2 accelerated in between those times and CME3 front was first identified at 08:30 UT. Black arrow points to the bubble-like structure observed behind CME3

Fig. 4 The Fig 4a: At 10:42 UT on 27 September 2001 the CME1 leading front (dashed blue line) was no longer visible after this time, CME1 core (dashed yellow line), CME2 (dashed red line), CME3 (dashed purple line). Fig 4b: Wind WAVES radio spectrum shows the second radio type II burst enhancement



tral angle of 189 degrees (similar to CME1), CME3 exhibited an initial speed of about 400 km s^{-1} , gradually accelerating. The last measured speed reached approximately 1000 km s^{-1} at a height of $30 R_{\odot}$. Notably, both CME2 and CME3 commenced acceleration upon reaching a height of $5 R_{\odot}$, with CME2's initial acceleration suggesting that CME3 did not act as a causal factor. The evolution of these CMEs and the occurrence of four distinct periods of radio enhancements in decameter-hectometric (DH) wavelengths are visually presented in Figs. 2–6.

5 Radio emissions

The dynamic spectrum depicted in Fig. 7 illustrates the radio data intensity measured by all receivers of the WAVES experiment onboard the Wind spacecraft, starting from 07:00 UT on September 27, 2001. While the AR was visible in decimeter-meter waves, no metric type II signals were identified in the spectrum. However, persistent and robust type III frequency drifting activity was observed throughout the entire day.

Fig. 5 The Fig 5a shows later evolution of CME2 (dashed red line), CME3 (dashed purple line), and the structure believed to still be the CME1 core (dashed yellow line) on 27 September 2001. Fig 5b: The radio emission frequency at that time was around 700 kHz which would have indicated a source height of about 12.6 R_{\odot} if calculated with the hybrid atmospheric density model

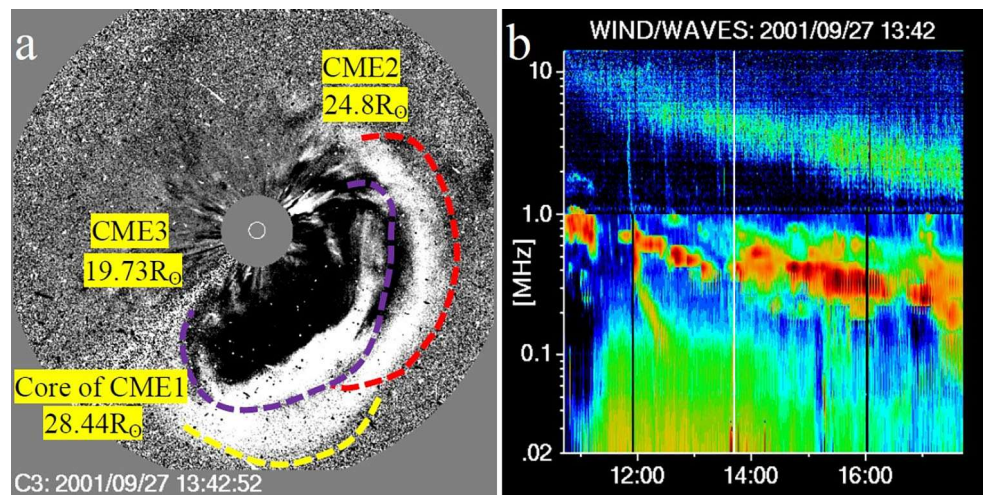
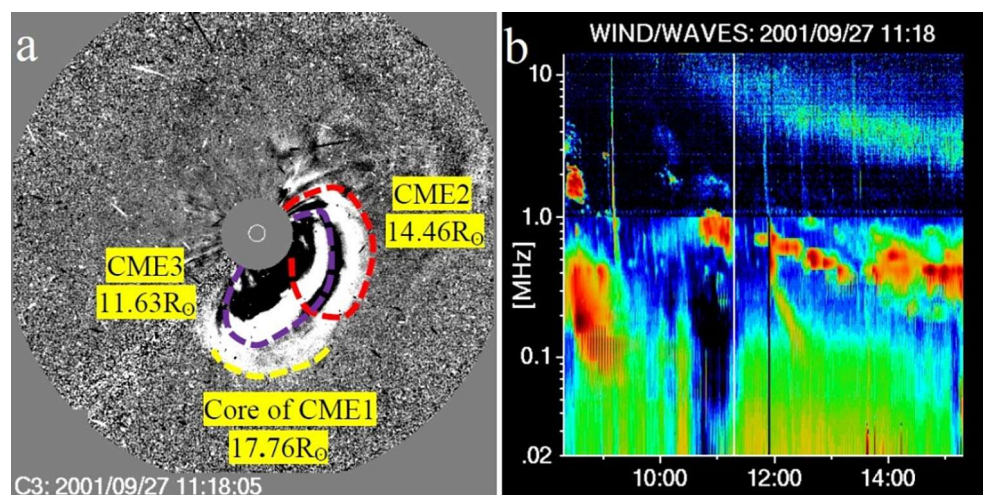


Fig. 6 The Fig 6a shows CMEs front locations at 13:42 UT on 27 September. Fig 6b: Shortly after this time the radio emission jumps to a higher frequency, to about 550 kHz, which indicates a source height of about 14.6 R_{\odot} if calculated with the hybrid density model. The emission lane also gets wider, which brings uncertainty to height estimates



The IP type II radio emission, highlighted by numbers (1-4) in Fig. 7, manifested during distinct periods: 1) 08:20–08:40 UT, 2) 10:40–11:20 UT, 3) 12:00–13:20 UT, and 4) 14:00–17:00 UT. Alongside these type II bursts, Wind/WAVES also recorded numerous short-lived type III-like bursts, known as a type III storm. fronts The CMEs reached the LASCO C3 field of view limits just after 14:00 UT. Consequently, a comparative analysis between radio and white-light structures became unfeasible beyond that time.

Figure 8 shows the predicted heights of the CME leading fronts and cores as a function of time, together with the computed radio source heights obtained using the hybrid and Leblanc models. The full-widths at half-maximum (FWHM) bandwidths of the radio emission are represented by the error bars connected to the radio heights as in Fig. 9. The type II frequencies are the lane centres, obtained as the peak frequencies of Gaussian fits. The peak frequencies as function of time are presented in Fig. 9. Here the error bars are the FWHM of the Gaussian distributions. Instantaneous

relative bandwidths were calculated by dividing the FWHM by the peak frequency at the corresponding time.

6 Height estimates of features

The manifestation of radio emission is contingent upon the electron plasma density (n_e , in cm^{-3}) in the source region, which diminishes as one moves away from the sun. The emission at decreasing frequencies is generated by a CME or shock traversing through the solar corona and IP space. Radio type II bursts, resulting from these shocks, generate emission at the fundamental or second harmonic frequencies, or both.

From the plasma frequency, the characterization of changes in electron density over time becomes feasible. This, in turn, enables the calculation of radio heights via coronal density models, contingent on the electron plasma density, which is dependent on coronal conditions. Widely utilized models include (Newkirk 1961; Saito 1970). The Newkirk model, hydrostatic at large distances from the sun,

Fig. 7 Wind/WAVES dynamic spectrum from 07:00 UT until the end of the day on 27 September 2001 shows the frequency range of 14 MHz–100 kHz. Type II emission periods are marked with numbers 1–4 and the emission lane centers are indicated with white lines

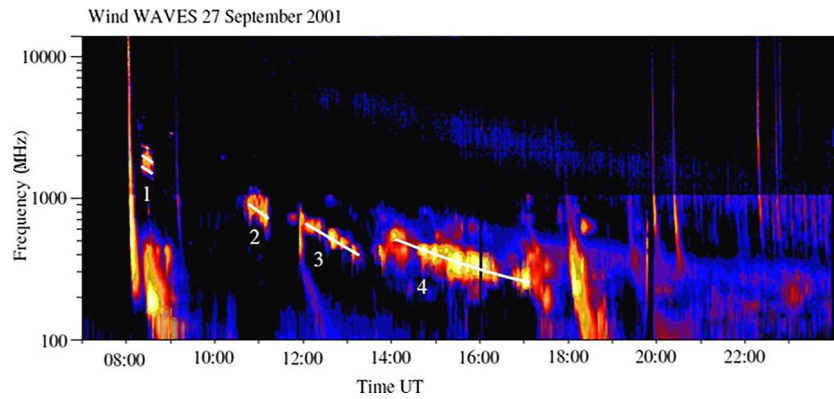


Fig. 8 Height evolution of the different features observed on 27 September 2001. The radio enhancement heights have been calculated using the hybrid atmospheric density model. Figure 9. Emission peak positions obtained from Gaussian fits. The points are 2-minute averages for the first period, and 5-minute averages for the others. The error bars are the FWHM bandwidth values

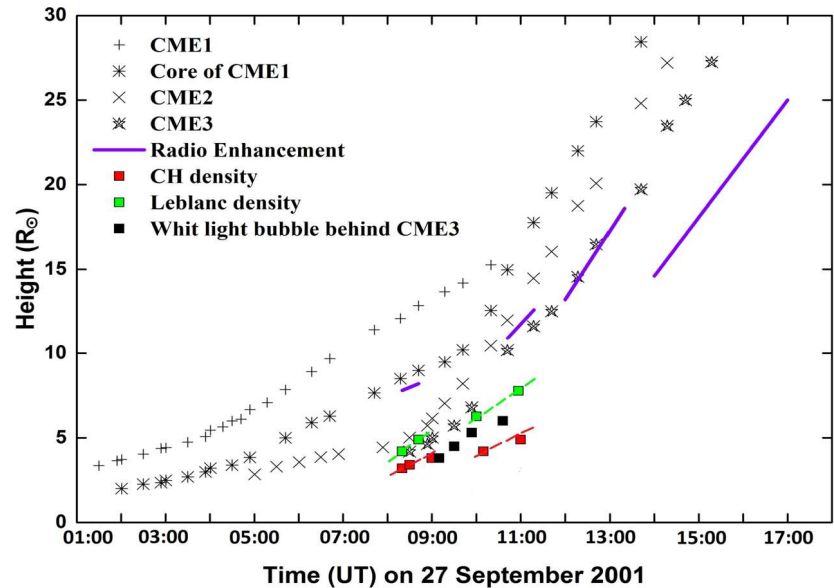
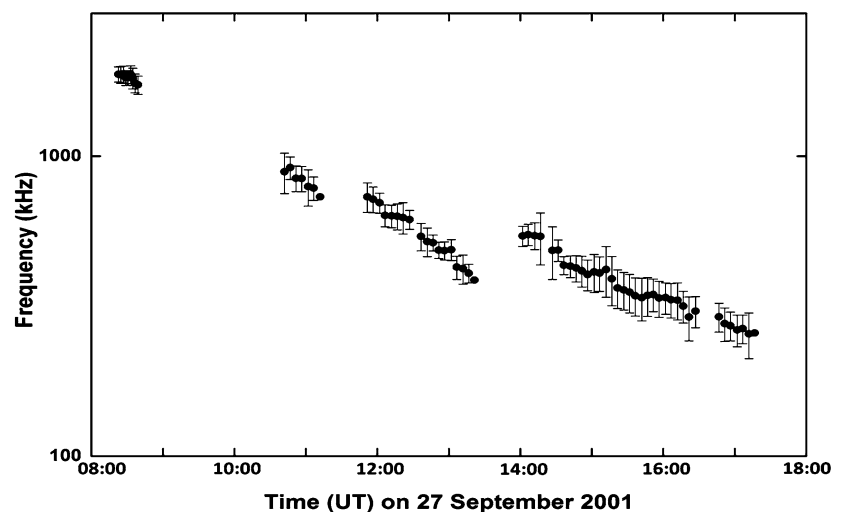


Fig. 9 Emission peak positions obtained from Gaussian fits. The points are 2-minute averages for the first period, and 5-minute averages for the others. The error bars are the FWHM bandwidth values



sustains high electron density numbers, posing inconsistency with (Mann et al. 2003, 1999), wherein corona density is significantly higher compared to IP space near 1 AU.

The (Saito 1970) model determines electron density values in IP space, while (Saito et al. 1977) suggests that at large distances, densities become close to $n_e \sim R^2$. The

Leblanc model provides densities for the low corona and IP space, valid for $R > 1.2 R_{\odot}$ but not for $R < 1.2 R_{\odot}$. Characterized by $n_e \propto R^{-2}$, this model yields an electron density of 7.2 cm^{-3} near 1 AU at larger distances ($R > 30 R_{\odot}$). The hybrid density model, introduced by (Vršnak et al. 2004) seamlessly combines high-density low-corona models and low-density IP models, essentially combining a five-fold (Saito 1970; Leblanc et al. 1998) models with minor modifications without breaks or discrepancies.

The hybrid density model is initially employed for the type II bursts lane and to calculate the heights of radio enhancements. Other density models are subsequently used to estimate the height of the radio source and compare them with CME heights Fig. 8. At 08:20 UT, the radio burst, superimposed with bright emission, lasted about 20 minutes, observing both fundamental and harmonic frequencies. The leading fronts of the three CMEs at the start time of the radio burst were at heights 12.1, 5.0, and $< 4.2 R_{\odot}$. The plasma density in the source region of the radio burst, measured at $3.36 \times 10^2 \text{ cm}^{-3}$, would be comparable to polar region densities if assumed to originate from heights of 4.0–5.0 R_{\odot} where CME2 and CME3 fronts were located (refer to Fig. 1 in (Pohjolainen et al. 2007)). Estimates for CME cavities suggest electron depletion ranging from 25% to 50% of mean coronal densities (Marqu'e 2004). However, at heights of 4.0–5.0 R_{\odot} , the densities would be around $4.0\text{--}2.0 \times 10^5 \text{ cm}^{-3}$, and even a depletion of 50% would not produce a density of $\sim 3.0 \times 10^4 \text{ cm}^{-3}$. The question arises whether such low densities could be present in the wake of CME1, assuming either CME2 or CME3 as the driver of the shock wave. It would be challenging for the shock to form and spread in such low densities, given that the local Alfvén speed would similarly rise. It became known that the shocks driven by CME produce type II radio emission in DH wavelengths e.g., (Reiner et al. 2000). The radio emission observed at the fundamental and/or second harmonic of plasma frequency its a result of accelerated electrons via CME driven shock. One shock wave arrived to the Earth on 29 September 2001 at 09:29 UT, 09:06 UT, and 09:03 UT observed by Wind, ACE, and SOHO/CELIAS respectively.

7 Shock wave arrival

It has been established that shocks induced by CMEs generate type II radio emission in DH wavelengths (Reiner et al. 2000). This radio emission, observed at the fundamental and/or second harmonic of the plasma frequency, results from the acceleration of electrons via CME-driven shocks. Three shock waves reached Earth on September 29, 2001, at 09:29 UT, 09:06 UT, and 09:03 UT, as observed by Wind, ACE, and SOHO/CELIAS, respectively. The first radio enhancement exhibited low density, CME3 essentially

penetrated the western side of CME2 because the cavity of CME1 had low density. At 8:20 UT, when the first type II signature appeared, the cavity was already at a considerable distance. This indicates that the shock formed via CME1. If the shock had formed due to the acceleration of CME2 or CME3, we would observe the cavity in front of them at lower heights.

The first enhancement's frequency drift at 08:20 UT is attributed to a shock wave generated by reconnection of field lines, accelerating both CME2 and CME3. There is also a possibility that the first period when the radio enhancement started at 08:20 UT is not connected to the second period when the radio enhancement began at 10:40 UT, given the substantial time gap without any emission. This suggests that the first type II radio emission represents a separate shock. In such a scenario, several explanations are plausible. The two shocks may be merging to produce a fast and robust shock (Wu et al. 2007). Alternatively, the preceding CME-driven shock could excite Alfvén waves and reinforce the turbulence region of the second or primary CME-driven shock. This would result in the second shock experiencing an increase in its seed population via pre-shock conditions.

Another possibility is the existence of two independently propagating shocks in different directions and with different densities. However, the second and third possibilities can be ruled out, as only one shock wave was observed near Earth on September 29. Furthermore, the rising phase of energetic particles occurred on September 25, with particles in the deceleration phase on September 27.

8 Discussion and conclusion

We examine the event on September 27, 2001, as an extraordinary occurrence where radio type II bursts were associated with three sequential CMEs, all originating from the same active regions. These CMEs were linked to solar flares with remarkably low density. The type II radio bursts were identified in the DH wavelength range and persisted into the kilometeric wavelength. Despite the visibility of the active region in the decimeter-meter wavelength, the spectra did not contain any metric type II signatures.

The first enhancement signals very low density, suggesting the presence of a low-density element. As we elucidated, CME1 exhibits a typical structure, with the core having low density. Consequently, CME3 essentially infiltrates the western side of CME2 due to the cavity having low density. By 08:20 UT, when the first type II burst appears, the cavity is already at a considerable distance. If the shock were formed by the acceleration of CME2 or CME3, the cavity would be observable in front of them at low heights. Additionally, the speed of the CME1 core is too slow to generate a shock wave. The first radio enhancement is attributed to a

shock wave initiated by reconnecting field lines, accelerating CME2 and CME3. This shock propagates sideways, as indicated by the small frequency drift. Low density could be explained if the shock were at the front of CME3, propagating either toward the CME2 cavity or inside a coronal hole visible above and below the active region-belt on the solar disk.

The subsequent radio enhancement occurs at 10:40 UT, matching the height of CME2, with a velocity of 650 km s^{-1} . The second radio enhancement aligns with the time when the CME1 core starts propagating faster, likely pushed by CME2. Enhanced radio emission could be created by the type II shock meeting with filament material. The third enhancement at 12:00 UT corresponds to the height of CME3, also with a velocity of 650 km s^{-1} . These third radio enhancements seem to be at the leading edge of CME3, with heights agreeing when using standard atmospheric models. These enhancements may be caused by irregularities in the solar wind plasma resulting from earlier transients (Knock et al. 2003).

Observing the height-time plot with the marked core front velocity reveals a change after 10 UT, and around 10:40, the core front passes the CME1 leading front. The fastest propagating part of CME3 catches the back part of the CME1 core at 09:24 UT and pushes CME2. By 09:18 UT, the core front is at a height of $8.8 R_{\odot}$, while CME3 is then at a height of $5.5 R_{\odot}$, pushing the rear end of the CME1 core.

The fourth enhancement experiences a jump to higher frequencies, indicating increasing density along the propagation path. This suggests merging densities of the CME1 core and CME2 within the propagation path of CME3.

In summary, our findings can be outlined as follows:

- The first radio enhancement is attributed to a shock wave initiated by the reconnecting field lines, propelling CME2 and CME3. This shock may be propagating sideways, indicated by a small frequency drift. The observed low density could be explained if the shock originated at the front of CME3, propagating either toward the CME2 cavity or inside a coronal hole.
- The second radio enhancement manifests near the time when the CME1 core accelerates, likely propelled by CME2. The heightened radio emission could result from the type II shock encountering filament material.
- The third radio enhancements seem to align with the leading edge of CME3, with heights consistent when using standard atmospheric models. These enhancements are likely induced by irregularities in the solar wind plasma resulting from earlier transients (Knock et al. 2003).
- The fourth enhancement exhibits a shift to higher frequencies, indicative of increasing density along the propagation path. This suggests the merging densities of the CME1 core and CME2 within the propagation path of CME3.

Acknowledgements We extend our sincere appreciation to the University of Basrah, College of Science, Department of Physics, and the Ministry of Higher Education and Scientific Research of Iraq for their invaluable support. Special thanks to the dedicated contributors involved in the creation and continuous updates of various solar event catalogues, laying the foundation for our research.

We acknowledge the CME Catalog, a collaborative effort between NASA, the Catholic University of America, and the Naval Research Laboratory, hosted and curated at the CDAW Data Center. The Wind WAVES radio type II burst catalogue, meticulously prepared by Michael L. Kaiser, finds its home at the Goddard Space Flight Center.

Furthermore, we recognize the significance of international cooperation embodied in the Solar and Heliospheric Observatory (SOHO), a joint project between the European Space Agency (ESA) and NASA. The collaborative spirit underlying these initiatives has been instrumental in advancing our understanding of solar phenomena.

Author contributions Firas Al-Hamadani and Amjad Al-Sawad both made equal contributions to the work

Data Availability No datasets were generated or analysed during the current study.

Declarations

Competing interests The authors declare no competing interests.

References

- Al-Hamadani, F., Pohjolainen, V.E.: Formation of radio type II bursts during a multiple coronal mass ejection event. *Sol. Phys.* **292**, 183 (2017). <https://doi.org/10.1007/s11207-017-1208-y>
- Bougeret, J.-L., Kaiser, M.L., Kellogg, P.J., Manning, R., Goetz, K., Monson, S.J., Monge, N., Friel, L., Meetre, C.A., Perche, C., Sitruk, L., Hoang, S.: WAVES: the radio and plasma wave investigation on the wind spacecraft. *Sci. Rev. Chem. Commun.* **71**, 231 (1995). <https://doi.org/10.1007/BF00751331>
- Cane, H.V., Sheeley, N.R. Jr., Howard, R.A.: Energetic interplanetary shocks, radio emission, and coronal mass ejections. *J. Geophys. Res.* **92**, 9869 (1987). <https://doi.org/10.1029/JA092iA09p09869>
- Cremades, H., Cyr St., O.C., Kaiser, M.L.: A tool to improve space weather forecasts: kilometric radio emissions from Wind/WAVES. *Space Weather* **5**, 8001 (2007). <https://doi.org/10.1029/2007SW000314>
- Delaboudinière, J.-P., Artzner, G.E., Brunaud, J., Gabriel, A.H., Hochedez, J.F., Millier, F., Song, X.Y., Au, B., Dere, K.P., Howard, R.A., Kreplin, R., Michels, D.J., Moses, J.D., Defise, J.M., Jamar, C., Rochus, P., Chauvineau, J.P., Marioge, J.P., Catura, R.C., Lemen, J.R., Shing, L., Stern, R.A., Gurman, J.B., Neupert, W.M., Maucherat, A., Clette, F., Cugnon, P., van Dessel, E.L.: EIT: extreme-ultraviolet imaging telescope for the SOHO mission. *Solar Phys.* **162**, 291 (1995). <https://doi.org/10.1007/BF00733432>
- Gary, D.E., Dulk, G.A., House, L., Illing, R., Sawyer, C., Wagner, W.J., McLean, D.J., Hildner, E.: *Astron. Astrophys.* **134**, 222 (1984)
- Gopalswamy, N., Kaiser, M.L., Thompson, B.J., Burlaga, L.F., Szabo, A., Lara, A., Vourlidas, A., Yashiro, S., Bougeret, J.-L.: Radio-rich solar eruptive events. *GeoRL* **27**, 1427 (2000). <https://doi.org/10.1029/1999GL003665>
- Klassen, A., Bothmer, V., Mann, G., Reiner, M.J., Krucker, S., Vourlidas, A., Kunow, H.: Solar energetic electron events and coronal shocks. *A & A* **385**, 1078 (2002). <https://doi.org/10.1051/0004-6361:20020205>

- Knock, S.A., Cairns, I.H., Robinson, P.A., Kuncic, Z.: Theoretically predicted properties of type II radio emission from an interplanetary foreshock. *J. Geophys. Res. Space Phys.* **108**, 1126 (2003). <https://doi.org/10.1029/2002JA009508>
- Kumar, P., Innes, D.E., Cho, K.-S.: Flare-generated shock wave propagation through solar coronal arcade loops and an associated type II radio burst. *Astrophys. J.* **828**, 28 (2016). <https://doi.org/10.3847/0004-637X/828/1/28>
- Leblanc, Y., Dulk, G.A., Bougeret, J.-L.: Tracing the electron density from the corona to 1 au. *Sol. Phys.* **183**, 165–180 (1998). <https://doi.org/10.1023/A:1005049730506>
- Mann, G., Jansen, F., MacDowall, R.J., Kaiser, M.L., Stone, R.G.: A heliospheric density model and type III radio bursts. *Astron. Astrophys.* **348**, 614 (1999)
- Mann, G., Klassen, A., Aurass, H., Classen, H.-T.: Formation and development of shock waves in the solar corona and the near-sun interplanetary space. *Astron. Astrophys.* **400**, 329 (2003). <https://doi.org/10.1051/0004-6361:20021593>
- Marqu'e, C.: Radio metric observations of quiescent filament cavities. *Astrophys. J.* **602**, 1037 (2004). <https://doi.org/10.1086/381085>
- Newkirk, G. Jr.: The solar corona in active regions and the thermal origin of the slowly varying component of solar radio radiation. *Astrophys. J.* **133**, 983 (1961). <https://doi.org/10.1086/147104>
- Pohjolainen, S., van Driel-Gesztelyi, L., Culhane, J.L., Manoharan, P.K., Elliott, H.A.: CME propagation characteristics from radio observations. *Sol. Phys.* **244**, 167 (2007). <https://doi.org/10.1007/s11207-007-9006-6>
- Reiner, M.J., Kaiser, M.L., Plunkett, S.P., Prestage, N.P., Manning, R.: Radio tracking of a white-light coronal mass ejection from solar corona to interplanetary medium. *Astrophys. J. Lett.* **529**, L53 (2000). <https://doi.org/10.1086/312446>
- Saito, K.: *Ann. Tokyo Astron. Obs.* **12**, 51 (1970)
- Saito, K., Poland, A.I., Munro, R.H.: A study of the background corona near solar minimum. *Sol. Phys.* **55**, 121 (1977). <https://doi.org/10.1007/BF00150879>
- Smerd, S.F., Sheridan, K.V., Stewart, R.T.: Split-band structure in type II radio bursts from the Sun. *Astrophys. Lett.* **16**, 23 (1975)
- Tsuneta, S., Acton, L., Bruner, M., Lemen, J., Brown, W., Carvalho, R., Catura, R., Freeland, S., Jurcevich, B., Morrison, M., Ogawara, Y., Hirayama, T., Owens, J.: The soft X-ray telescope for the SOLAR-a mission. *Sol. Phys.* **136**, 37 (1991). <https://doi.org/10.1007/BF00151694>
- Vršnak, B., Magdalenic, J., Zlobec, P.: Band-splitting of coronal and interplanetary type II bursts. *Astron. Astrophys.* **413**, 753 (2004). <https://doi.org/10.1051/0004-6361:20034060>
- Webb, D.F., Howard, T.A.: Coronal mass ejections: observations. *Living Rev. Sol. Phys.* **9**, 3 (2012)
- Wild, J.P.: *Radiotekhnika*, 1 (1963)
- Wu, C.-C., Fry, C.D., Dyer, M., Wu, S.T., Thompson, B., Liou, K., Feng, X.S.: Three-dimensional global simulation of multiple ICME interaction and propagation from the Sun to the heliosphere following the 25 28 October 2003 solar events. *Adv. Space Res.* **40**, 1827 (2007). <https://doi.org/10.1016/j.asr.2007.06.025>

Publisher's Note Springer Nature remains neutral with regard to jurisdictional claims in published maps and institutional affiliations.

Springer Nature or its licensor (e.g. a society or other partner) holds exclusive rights to this article under a publishing agreement with the author(s) or other rightsholder(s); author self-archiving of the accepted manuscript version of this article is solely governed by the terms of such publishing agreement and applicable law.